Investigation of the Stereodefect Distribution and Conformational Behavior of Isotactic Polypropylene Polymerized with Different Ziegler–Natta Catalysts

Jian Kang, Feng Yang, Tong Wu, Huilin Li, Dongming Liu, Ya Cao, Ming Xiang

State Key Laboratory of Polymer Materials Engineering, Polymer Research Institute of Sichuan University, Chengdu 610065, People's Republic of China

Received 8 July 2011; accepted 11 October 2011
DOI 10.1002/app.36357
Published online 1 February 2012 in Wiley Online Library (wileyonlinelibrary.com).

ABSTRACT: Two isotactic polypropylene (iPP) samples (PP-A and PP-B) were obtained by utilizing two different heterogeneous Ziegler–Natta catalysts in a given polymerization system. The molecular structure and conformational behavior of the samples were studied. The results of determination of xylene soluble material (XS) and ^{13}C NMR showed that the average isotacticity of the samples were nearly same. However, the results of high-resolution high-temperature ^{13}C NMR (HRHT ^{13}C NMR) and successive self-nucleation and annealing (SSA) fractionation revealed that the amount of high isotacticity of PP-B was lower than that of PP-A, and the amount of relative medium and low isotacticity of PP-B was higher than PP-A, indicating that the stereodefect distribution of PP-B was more uniform than PP-A. The calculation of average meso sequence length from SSA was found to be in good agreement with that calculated from the results of HRHT ^{13}C NMR. Moreover, Fourier transformation infrared was utilized to study the influence of stereodefect distribution on the conformational behavior of iPP. The result suggested that the molecular conformation of the PP-B was more disordered than PP-A, the regularity of molecular structure for PP-B was lower than that of PP-A. The related action mechanism and the influences of which on crystallization behavior were discussed. © 2012 Wiley Periodicals, Inc. J Appl Polym Sci 125: 3076–3083, 2012

Key words: isotactic polypropylene; stereodefect distribution; conformation

INTRODUCTION

Because heterogeneous Ziegler–Natta catalysts contain multiple active sites, the polypropylene resins produced usually have varying degree and distribution of stereoregularity. The average isotacticity, and the distribution of stereodefects and stereoregular sequences in the formed polymer are the most revealing structure information related to the catalyst and the polymerization mechanism of polypropylene,[1,2] which also determines for most part of the crystallization behaviors, processability and mechanical properties. If the characterization of the average isotacticity and the stereodefect distribution of isotactic polypropylene (iPP) can be done thoroughly enough, information on the catalyst, crystallization behavior, and mechanical properties is gained as well.

In the characterization of stereodefect distribution of iPP, solvent fractionation[3–8] (usually an extremely time consuming and tedious work), high-resolution high-temperature ^{13}C NMR (HRHT ^{13}C NMR), temperature rising elution fractionation,[7] crystallization analysis fractionation,[3,10–13] crystallization elution fractionation,[14,15] and thermal fractionation methods are often used. Among which, the thermal fractionation methods, such as stepwise isothermal crystallization[16–19] and successive self-nucleation and annealing (SSA),[16,20–23] are increasingly used in analyzing the microstructure of polyolefin, due to their enhanced resolution, effective molecular segregation, relatively short measurement times, free of solvent, and additional molecular structural information.

On the other hand, the stereodefects places in the polypropylene molecules, influences the movement of the macromolecules and might affect on the folding manner and helical conformation of iPP. Conversely, if the conformational behavior of iPP could be studied, the information of the stereodefect distribution might also be revealed. However, few studies had concerned on the relationship between the distribution of stereodefects and the conformational behavior of iPP. Fourier transformation infrared (FT-IR) spectroscopy is an effective method for characterizing the helical conformation behavior of iPP.[24–27] During the past decades, the relationship between specific regularity bands of FT-IR spectrum and the different critical helix length "*n*" of iPP had been established.[28–34] The IR bands at 940, 1220, 1167, 1303, 1330, 840, 998, 900, 808, 1100, and 973 cm^{-1}

Correspondence to: Y. Cao (Caoya@scu.edu.cn) or M. Xiang (xiangming45@hotmail.com).

correspond to helical structures with degree of order from high to low, and the minimum n values for appearance of bands at 973, 998, 840, and 1220 cm^{-1} are 5, 10, 12, and 14 monomers units in helical sequences, respectively. Obviously, larger n value corresponds to higher ordered degree of the corresponding regularity.

The aim of this study is to investigate the influence of different Ziegler–Natta catalysts on the molecular structure, especially the stereodefect distribution of iPP, and the relationship between the stereodefect distribution and the conformational behavior of the iPP. Two commercial heterogeneous Ziegler–Natta catalysts were used in a given polymerization system, and the other polymerization conditions remained constant. The molecular structure of the iPP samples obtained was investigated by Differential scanning calorimetry (DSC), determination of xylene soluble material (XS), ^{13}C NMR and SSA fractionation. Moreover, FT-IR was used to study the conformational behavior of the samples. The relationship between the conformational behavior and the distribution of stereodefects of the iPP samples were studied, and the resulting influence on crystallization behavior was discussed.

EXPERIMENTAL

Materials

Samples studied in this article were iPP resins for biaxially oriented polypropylene film, produced in the Spheripol process (Basell) in the two loop reactors, which is one of the most widespread commercial methods to produce polypropylene.[35] The temperature for the prepolymerization reactor was controlled at 20°C and 70°C for the main polymerization reactors. The pressure of those three reactors ranged from 3.4 to 4.2 MPa. The cocatalyst was triethylaluminum (TEAL), and the external donor used was cyclohexylmethyldimethoxysilane (CHMDMS). The mole ratio of the cocatalyst/external donor (TEAL/CHMDMS, denoted as Al/Si in this study) was 40, and other conditions remained unchanged. Two different highly activity supported forth generation Ziegler–Natta ($TiCl_4 = MgCl_2$) catalysts, ZN-A and ZN-B, were used. Two samples, PP-A and PP-B were obtained during the polymerization.

Characterization

High-resolution high-temperature ^{13}C NMR

The HRHT ^{13}C NMR was performed with Bruker AVANCE 400 NMR spectrometer operating at 100.62 MHz for carbon. Samples was dissolved in 1,2,4-trichlorobenzene with 20% deuterated benzene in 10 mm BBO tubes. The experiments were performed at 120°C. All sequences round 21, 29, and 46 ppm were assigned according to the literatures.[36,37] Experimental conditions were number of pulses more than 10,000, pulse angle 30, spectrum width 25,000 Hz, and relaxation delay 7 s. All spectra were completely proton decoupled.

It should be noted that there usually exists an amount of very low tacticity and atacticity in the iPP samples, which might give a misleading influence on the tacticity distribution information obtained from HRHT ^{13}C NMR. As a result, the data of HRHT ^{13}C NMR might cannot reflect the exact distribution of stereodefects along the major molecular chains. To exclude the influence of this fraction, samples were extracted in n-heptane for 24 h at desired temperature, then, the insoluble fraction was dried and collected for the measurement.

Fourier transformation infrared spectroscopy

Samples were first molded into thin film using platen press at 200°C and the pressure of 10 MPa, then they were cooled down to ensure the same thermal history. The spectra were measured at 26°C using a Nicolet Magna 560 FT-IR spectrometer and collected at a resolution of 4 cm^{-1} with 16 scans. The range of measured wavenumber was 400–4000 cm^{-1}. All the original spectra were baseline corrected using OMNIC E.S.P software.

Differential scanning calorimetry

All the calorimetric experiments were carried out on Mettler Toledo DSC1 differential scanning calorimeter under nitrogen atmosphere (50 mL/min). Calibration for the temperature scale was performed using indium as a standard to ensure reliability of the data obtained. To ensure the homogeneity of samples and the good contact between sample and pan, the virgin polymer was molded at 190°C, 10 MPa for 5 min into sheets of uniform thickness about 500 μm. Then 5 mg round samples were punched out of the sheets.

Successive SSA fractionation

The complete thermal treatment of SSA fractionation comprises the following steps: (a) erasure of the crystalline thermal history by heating the sample to 200°C and held for 5 min; (b) cooling the sample at 20°C/min to 30°C and held for 2 min; (c) the sample was heated at 20°C/min from 30°C to a partial melting temperature denoted T_s; (d) the sample was kept at T_s for 15 min; (e) DSC cooling scan at 20°C/min from T_s to 30°C, where the effects of the thermal treatment will be reflected on the crystallization of the sample; (f) repeat step "c" to "e" at increasingly

TABLE I
Molecular Structural Parameters of PP-A and PP-B

Sample	Catalyst	Al/Si ratio	XS (%)[a]	Isotacticity (%)[b]	$\overline{M_n}$[c]	$\overline{M_w}$[c]	$\overline{M_w}/\overline{M_n}$[c]
PP-A	ZN-A	40	3.8	96.6	112,800	365,050	3.24
PP-B	ZN-B	40	3.9	96.4	95,600	347,150	3.63

[a] Xylene soluble fraction at room temperature according to ASTM D5492.
[b] Isotacticity were obtained from high-temperature ^{13}C NMR at 120°C.
[c] Molecular weight and distribution were performed by gel permeation chromatography at 130°C.

lower T_s, which were varied from 167 to 139°C at 4°C intervals for a total eight self-nucleation/annealing steps. (g) Finally, the sample was heated at 10°C/min from 30°C to 200°C, and a multiple melting endotherm was obtained.

The first T_s temperature to be used in step "d" was carefully chosen as 167°C, which was the lowest temperature within domain II (or self-nucleation Domain, defined by Fillon et al.[38–40]) of the iPP resin studied in this article.

RESULTS AND DISCUSSION

Preliminary molecular characterization

The average isotacticities of the samples were characterized using the determination of XS fraction according to ASTM D5492 and high-temperature solution ^{13}C NMR. The molecular weight and its distribution were measured by gel permeation chromatography. Detailed molecular characteristics were listed in Table I. The crystallization and melting results were obtained by DSC, which were shown in Figure 1 and Table II.

Table I shows that the amount of XSs and average isotacticity of the samples are nearly same, suggesting that the catalysts of ZN-A and ZN-B have similar influence in determining the average isotacticity, in the polymerization system used in this study.

However, the crystallization and melting results in Figure 1 and Table II show that the crystallization peak temperature T_c, onset crystallization temperature $T_{c\ onset}$, endset temperature of crystallization $T_{c\ endset}$, melting peak temperature T_m, and onset melting temperature $T_{m\ onset}$ of PP-A are all higher than that of PP-B, indicating the crystallizability of PP-A is stronger than PP-B. The differences in crystallization and melting temperatures of iPP are usually attributed to the different average isotacticities and/or different distributions of the stereodefects. Because the average isotacticities of the samples are nearly same, the different crystallization parameters might indicate that the stereodefect distributions of the samples are different. However, according to the analysis of XS and ^{13}C NMR, information on the stereodefect distribution can hardly be obtained, more detailed structural characterizations are required.

High-resolution high-temperature ^{13}C NMR

To investigate the stereodefect distribution of the samples, the HRHT ^{13}C NMR was performed. The original HRHT ^{13}C NMR spectra were shown in Figure 2.

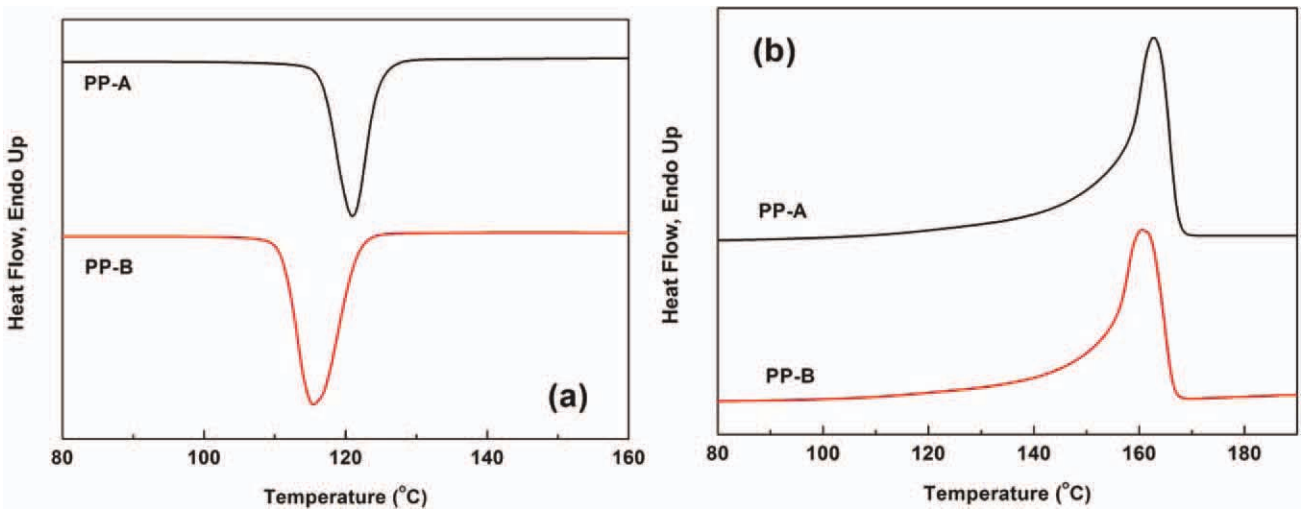

Figure 1 DSC (a)cooling curves and (b) subsequent heating curves. (Cooling and heating rates were 10°C/min). [Color figure can be viewed in the online issue, which is available at wileyonlinelibrary.com.]

TABLE II
Crystallization and Melting Parameters of PP-A and PP-B

	Cooling scan[a]			Subsequent heating scan[a]			
Sample	T_c (°C)	$T_{c\ \text{onset}}$ (°C)	$T_{c\ \text{endset}}$ (°C)	T_m (°C)	$T_{m\ \text{onset}}$ (°C)	$T_{m\ \text{endset}}$ (°C)	X_c (%)
PP-A	121.2	124.9	116.9	162.9	156.8	167.6	44.7
PP-B	114.6	119.9	110.7	159.2	152.5	167.3	41.3

[a] The cooling rate and subsequent heating rate were 10°C/min.

Table III shows the contents of the "*mmmm*," "*mmmr*" pentads of PP-B are lower than that of PP-A, meanwhile, the amounts of "*rmmr*," "*mr*," and "*rr*" of PP-B are all higher than PP-A. Namely, for ZN-B catalyst system, more stereoirregular insertion occurs during the polymerization process compared with ZN-A catalyst system. Because the average isotacticity of the samples are nearly same (Table I), the results in Table III indicate that, the stereospecificity of the two catalyst systems in determining the stereodefect distribution of iPP are different. Because of this, the different catalyst systems lead to different distribution of stereodefects: for ZN-B catalyst system, the stereodefect distribution of the resulting iPP is more uniform than that of ZN-A.

Successive SSA fractionation

SSA is an effective method in the characterization of the stereodefect distribution of iPP.[18,21] The SSA final melting curves of the samples are shown in Figure 3. According to the basic principle of SSA fractionation,[16] the SSA curve was fitted into nine individual peaks using Peakfit 4.12 software, including two main peaks in the high-temperature region and seven minor peaks in the low-temperature region, as can be seen from Figure 3. The main peak located at the highest temperature is denoted as peak1 and the followed main peak located at high temperature is peak2.

Figure 3 shows that the relative heights of the two main peaks on the SSA curves of PP-A and PP-B are quite different. Compared with PP-A, the relative height of peak1 of PP-B is obviously lower, whereas the relative height of peak2 is higher. According to the literatures,[20,23] peak1 corresponds to the melting of thick lamellae, which is crystallized by the molecules with high isotacticity; peak2 corresponds to medium thickness lamellae, which correspond to the fraction with relative medium isotacticity. It can be directly observed from the SSA curves that, compared with PP-A, PP-B has less amount of high

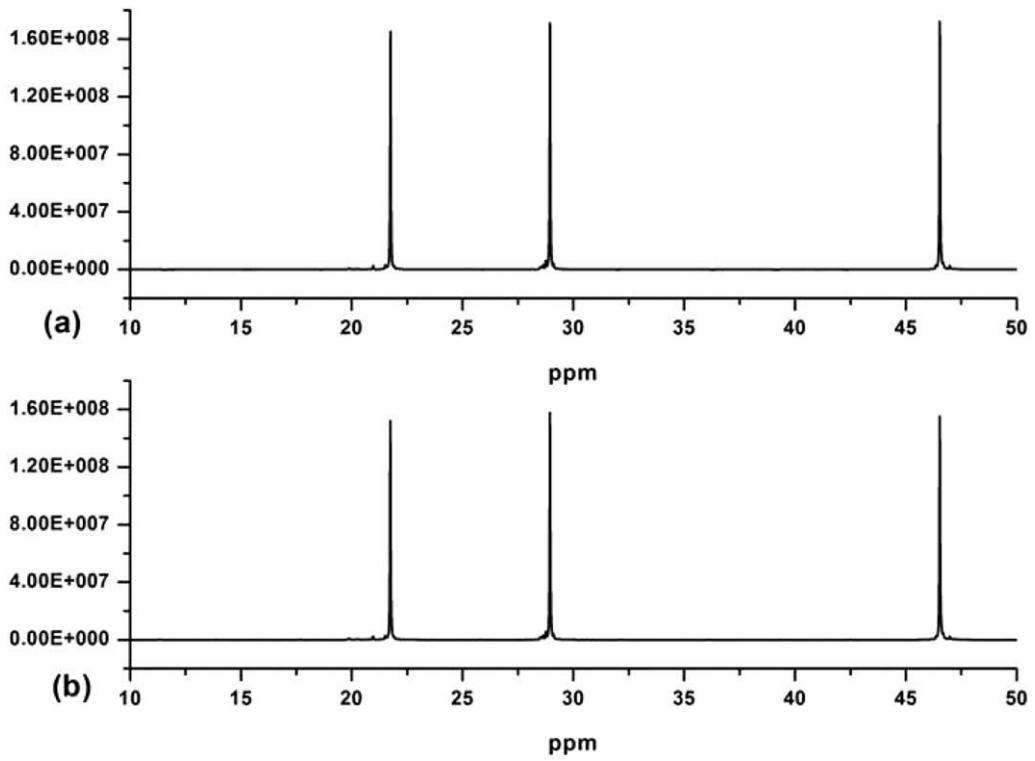

Figure 2 HRHT ^{13}C NMR spectrums of (a) PP-A and (b) PP-B.

TABLE III
Tacticity Results from HRHT ^{13}C NMR Analysis of PP-B and PP-A

	mm			*mr*				*rr*			
Sample[a]	*mmmm*	*mmmr*	*rmmr*	*mr*	*mmrr*	*mmrm + rmrr*	*rmrm*	*rr*	*rrrr*	*mrrr*	*mrrm*
PP-A	95.07	1.59	0.41	2.99	2.12	0.57	0.30	1.94	0.61	0.45	0.88
PP-B	94.78	1.47	0.53	3.19	2.17	0.71	0.31	2.03	0.65	0.48	0.90

[a] Samples were extracted in *n*-heptane for 24 h at desired temperature and then the insoluble fraction was collected and dried for HRHT ^{13}C NMR measurement, to exclude the influence of the atactic fraction.

isotacticity and more amount of relative medium isotacticity.

To obtain quantitative information, the relative area percentages (i.e., the integral area percentages on the SSA melting curve) of the peaks fitted from the SSA curve were calculated. The results are shown in Figure 4.

As can be seen from Figure 4, the relative area percentages of all the peaks of the samples, except peak1 and peak2, are very close; the relative area percentage of peak1 of PP-A is 7.7% higher than that of PP-B, whereas the relative content of peak2 is 9.2% lower than that of PP-B.

Using Thomson–Gibbs equation[41] [eq. (1)], information about the lamellar thickness distribution of iPP can be obtained:

$$T_m = T_m^{\prime 0}\left(1 - \frac{2\sigma}{\Delta H_0 L}\right) \quad (1)$$

where the equilibrium temperature $T_m^0 = 460$ K,[42,43] the melting enthalpy $\Delta H_0 = 184\times10^6$ J/m^3, and the surface free energy σ=0.0496 J/m^2.

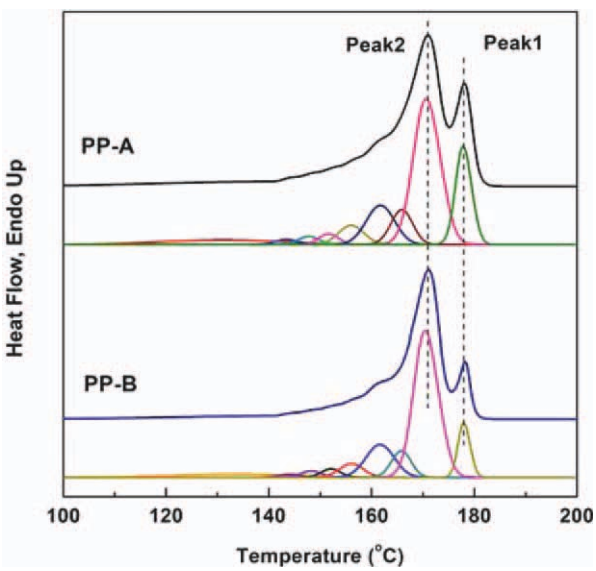

Figure 3 SSA final melting curves and the corresponding fitted curves of PP-A and PP-B. The melting peak locating at the higher temperature region is denoted as peak1 and the lower one peak2. [Color figure can be viewed in the online issue, which is available at wileyonlinelibrary.com.]

The lamellar thickness distribution curves of the samples are shown in Figure 5. Note that the intensities of the curves are normalized.

Figure 5 shows that there are two main peaks on the lamellar thickness distribution curve, which are denoted as peak1′ and peak2′, corresponded to peak1 and peak2 on the SSA curve, respectively. Compared with PP-A, the relative intensity of peak1′ for PP-B is obviously lower, whereas the relative intensity of peak2′ for PP-B is higher, indicating that after the same SSA thermal treatment, more amount of thick lamellae and less amount of thin lamellae have formed in PP-A.

Moreover, with the aim of evaluating the heterogeneity of the stereodefect distribution along the chains in a quantitative manner, a method using mathematical relationships that are analogous to those employed to describe molecular distributions in polymer and polydispersity.[44] The statistical parameters describing the lamellar thickness, the arithmetic average lamellar thickness L_n, the weighted average lamellar thickness L_w, are introduced and defined as follows:

$$L_n = \frac{n_1L_1 + n_2L_2 + n_3L_3 + n_4L_4 + , \ldots , + n_jL_j}{n_1 + n_2 + n_3 + n_4 + , \ldots , + n_j} = \sum f_iL_i \quad (2)$$

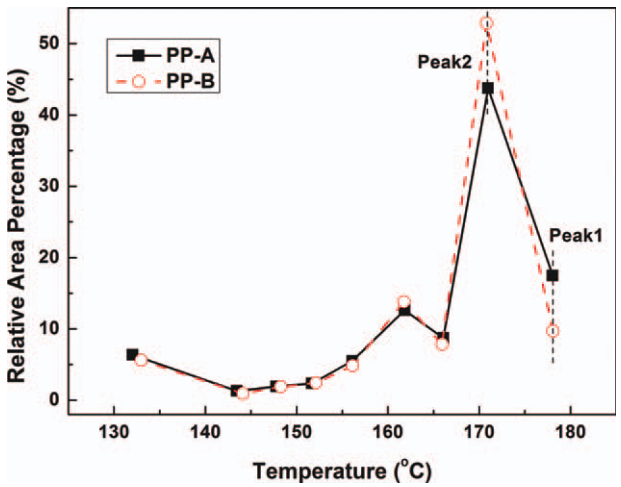

Figure 4 Relative area percentages of the peaks on the SSA curves of PP-A and PP-B. [Color figure can be viewed in the online issue, which is available at wileyonlinelibrary.com.]

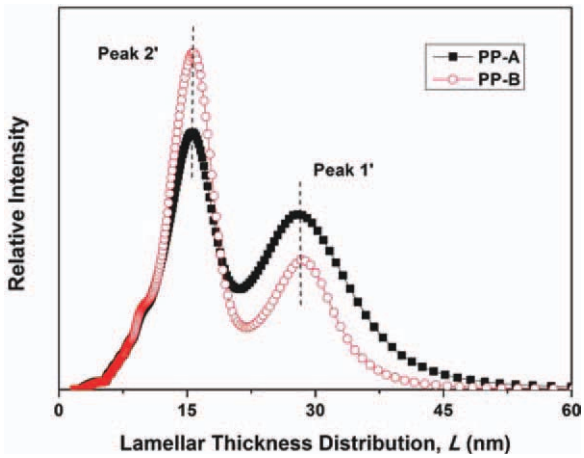

Figure 5 Lamellar thickness distribution curves of PP-A and PP-B, obtained by using Thomson–Gibbs equation on the SSA final melting curves. The intensities of the curves were normalized. [Color figure can be viewed in the online issue, which is available at wileyonlinelibrary.com.]

$$L_w = \frac{n_1 L_1{}^2 + n_2 L_2{}^2 + n_3 L_3{}^2 + n_4 L_4{}^2 + , \ldots , + n_j L_j{}^2}{n_1 L_1 + n_2 L_2 + n_3 L_3 + n_4 L_4 + , \ldots , + n_j L_j} = \frac{\sum f_i L_i{}^2}{\sum f_i L_i} \quad (3)$$

where n_i is the normalized partial area of the fractions on the final SSA curve, and the L_i is the lamellar thickness for each fraction.

Meanwhile, the broadness index (I) is defined as:

$$I = \frac{L_w}{L_n} \quad (4)$$

Furthermore, the arithmetic average meso sequence length (MSL_n, propylene unit) and weighted average meso sequence length (MSL_w, propylene unit), were calculated using eq. (5)[45]:

$$\mathrm{MSL} = 3L \Big/ L_{\mathrm{helix}} \quad (5)$$

where L is the lamellar thickness and L_{helix} is the length of one crystal cell along the chain direction. For the crystal cell of monoclinic form, the c-axis, which corresponds to chain direction, is 0.65 nm. In this direction, one cell contains 3 monomers,[46] $L_{\mathrm{helix}} = c = 0.65$ nm.

The average meso sequence length (m) was evaluated from the results of HRHT ^{13}C NMR using the following equation[47]:

$$m = \frac{mmmm + 3 * \frac{1}{2} mrrr + 2rmmr + \frac{1}{2} rmrm + \frac{1}{2} rmrr}{\frac{1}{2} rmrm + \frac{1}{2} rmrr + rmmr + \frac{1}{2} mmmr} \quad (6)$$

The results were calculated and listed in Table IV.

Table IV reveals that, the L_n and L_w of PP-A are larger than that of PP-B, indicating a larger average lamellar thickness of PP-A; the broadness index I of PP-A is larger than PP-B, suggesting that the distribution of lamellar thickness of PP-A is broader. As is studied above, the average isotacticity of the samples are nearly same (see Table I). Therefore, the results of SSA suggest that, compared with PP-A, PP-B has less amount of high isotacticity, more amount of relative medium isotacticity, and a more uniform distribution of the stereodefects.

On the other hand, from the calculation of average meso sequence length, it can be seen that the m and MSL_n are quite close, the MSL_w of the sample is larger than m and MSL_n; the variation of m, MSL_n and MSL_w are in good correspondence. In another word, the average meso sequence length calculated from SSA is in good agreement with that calculated from high-resolution ^{13}C NMR. SSA fractionation is effective in studying the stereodefects distribution of iPP polymerized with different heterogeneous Ziegler–Natta catalysts.

In general, the analysis of XS and ^{13}C NMR show that the average isotacticities of PP-A and PP-B are nearly same. According to HRHT ^{13}C NMR and SSA fractionation, it is found that the stereodefect distributions of the samples are quite different, the stereodefect distribution of PP-B is more uniform.

The different distributions of stereodefects along the molecular chains of the samples are attributed to the different Ziegler–Natta catalysts used. It is known that, there exist multiple active centers in heterogeneous Ziegler–Natta catalyst system, which are different from each other in stereospecificity and stability. For different catalyst systems, the activities of the active centers are quite different from each other. In study, the catalyst system of ZN-B is more preferred for the formation of a more uniform

TABLE IV
Lamellar Thickness Parameters, Arithmetic Average Meso Sequence Length (MSL_n), and Weighted Average Meso Sequence Length (MSL_w) Calculated From SSA, and the Average Meso Sequence Length (m) Calculated From ^{13}C NMR Results

Sample	L_w (nm)	L_n (nm)	$I = L_w/L_n$	MSL_w (propylene unit)	MSL_n (propylene unit)	m
PP-A	18.2	15.1	1.21	84.0	69.7	63.3
PP-B	16.5	14.2	1.16	76.2	65.5	58.9

insertion of the stereodefects along the molecular chains than that of ZN-A.

Fourier transformation infrared spectroscopy

In this section, the FT-IR measurement was performed to investigate the conformational behavior of the samples and the relationship between the stereodefect distribution and the conformational behavior of the iPP.

The original FT-IR spectra of the samples are shown in Figure 6. Because each IR band has its own intensity coefficient, it is necessary to normalize the intensities of these regular helical conformation bands. The IR band at 1460 cm^{-1}, which corresponds to the asymmetric deformation vibration of the methyl group, can serve as an internal standard, because it is almost not influenced by the variation of external environment.[25] To obtain better clarity, for both PP-A and PP-B, the normalized relative intensities of each regularity bands of PP-A were further taken as the references. The result is shown in Figure 7.

Figure 7 shows the relative intensities of the regularity bands at 973, 998, 840, and 1220 cm^{-1} of PP-B are all lower than that of PP-A, indicating that the relative contents of all length of helical sequences of PP-B are lower than that of PP-A, and the conformational order degree of PP-B is lower than PP-A.

Because the samples for FT-IR measurement have the same thermal history, the differences in conformation are attributed to the different molecular structural regularities of the samples. Because the average isotacticities (i.e., the amount of stereodefects) of PP-A and PP-B are nearly same, it can be concluded that the differences in conformational order degree are attributed to the different distribution of stereodefects of the samples. The stereodefects distributes on iPP molecular chains, restrains the cooperative movement of the repeating units and influences the folding manner of the chains, and thus decreases the helical conformational order degree of the iPP sample. The more uniform the distribution of stereodefects is, the lower the order degree of the helical conformation is.

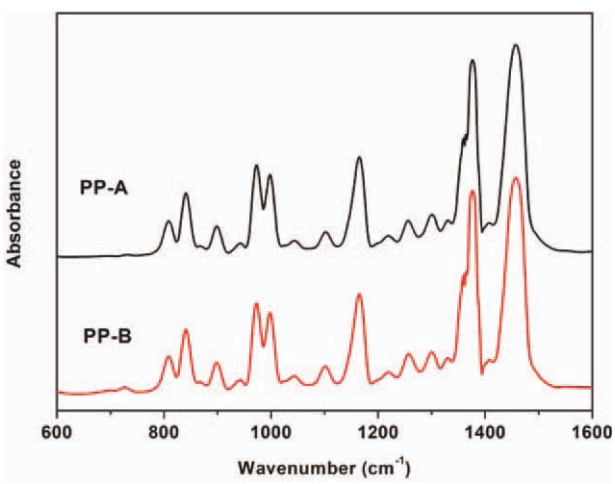

Figure 6 FT-IR spectra of PP-A and PP-B. [Color figure can be viewed in the online issue, which is available at wileyonlinelibrary.com.]

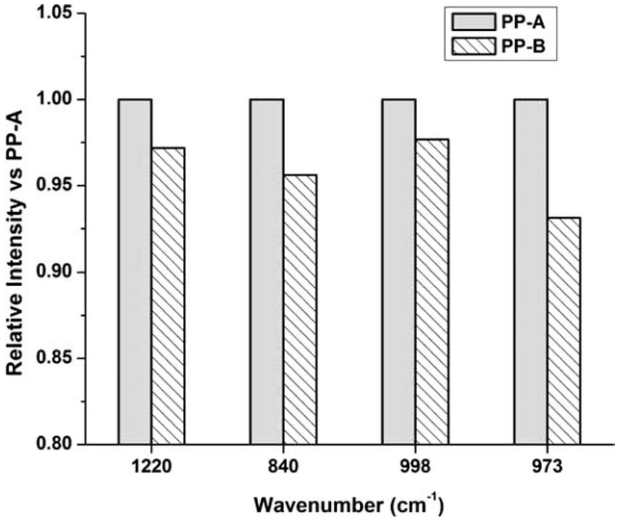

Figure 7 Relative intensities of different regularity bands of PP-A and PP-B. The intensities of all the bands of PP-A were taken as the reference.

Compared with PP-B, the conformational order degree of PP-A is higher, revealing that the regularity of the molecular chains for PP-A is higher. This result is coincident with the results of HRHT ^{13}C NMR and SSA. Therefore, the manner of stereodefect distribution determines the conformational order degree of iPP. FT-IR can be applied to study the distribution of stereodefects of iPP from the conformational aspect. Moreover, it is found that the catalyst system of ZN-B is more preferred for the formation of iPP with lower degree of conformational order than that of PP-A.

On the aspect of crystallization, the study of Zhu et al.[34] conformed that, when the persistence length of 3_1 helical sequences exceeded 12 monomer units (corresponding to the emergence of regularity bands at 840 cm^{-1}), the iPP melt system will be unstable, and the 3_1 helix conformation extends quickly and then the crystallization occurs. Interestingly, in this study, the amounts of the regularity bands of 840 and 1220 cm^{-1} of PP-A are all higher than that of PP-B (in the same thermal treatment), which might indicate that the crystallizability of PP-A is stronger than that of PP-B. The crystallization and melting parameters in Table II is in agreement with this speculation.

CONCLUSIONS

In this study, the average isotacticity, stereodefect distribution and conformational behavior of the iPP

resins polymerized with different Ziegler–Natta catalysts were studied.

The results of XS, ^{13}C NMR showed that the average degree of tacticity of PP-A and PP-B are similar, suggesting that the catalysts of ZN-A and ZN-B have similar influence in determining the average isotacticity in the polymerization system used in this study.

The analysis of HRHT ^{13}C NMR and SSA suggested that compared with PP-B, the amount of high-isotacticity component of PP-A is higher, the amount of relative medium and low-isotacticity component of PP-A is lower, the distribution of stereodefects of PP-B is more uniform. The calculation of weighted average meso sequence length from SSA was found to be in good agreement with that calculated from the results of HRHT ^{13}C NMR. The catalyst system of ZN-B was found to be preferred for the formation of more uniform distribution of stereodefects than ZN-A catalyst system.

The results of FT-IR showed that the conformational order degree of PP-B is lower than that of PP-A, indicating that the stereodefect distribution is one of the crucial factors on the conformational order degree of iPP. FT-IR is effective in reflection of the differences in stereodefect distribution of the samples from the conformational aspect. Moreover, the catalyst system of ZN-B is more preferred for the formation of iPP with lower degree of conformational order than that of PP-A.

References

1. Viville, P.; Daoust, D.; Jonas, A. M.; Nysten, B.; Legras, R.; Dupire, M.; Michel, J.; Debras, G. Polymer 2001, 42, 5, 1953.
2. Soares, J. B. P. Chem Eng Sci 2001, 56, 4131.
3. Xu, J.; Feng, L.; Yang, S.; Yang, Y.; Kong, X. Eur Polym J 1998, 34, 431.
4. Ogawa, T.; Hoshino, S. J Appl Polym Sci 1973, 17, 2235.
5. Kawamura, H.; Hayashi, T.; Inoue, Y.; Chujo, R. Macromolecules 1989, 22, 2181.
6. Paukkeri, R.; Iiskola, E.; Lehtinen, A.; Salminen, H. Polymer 1994, 35, 2636.
7. Paukkeri, R.; Vaananen, T.; Lehtinen, A. Polymer 1993, 34, 2488.
8. Lehtinen, A.; Paukkeri, R. Macromol Chem Phys 1994, 195, 1539.
9. Dong, Q.; Wang, X.; Fu, Z.; Xu, J.; Fan, Z. Polymer 2007, 48, 20, 5905.
10. Anantawaraskul, S.; Soares, J. B. P. Adv Polym Sci 2005, 182, 1.
11. Soares, J. B. P.; Anantawaraskul, S. J Polym Sci Part B: Polym Phys 2005, 43, 1557.
12. Wijga, P. W. O.; Van Schooten, J.; Boerma, J. Macromol Chem 1960, 36, 115.
13. Xu, J. T.; Feng, L. X. Eur Polym J 2000, 36, 867.
14. Monrabal, B.; Sancho-Tello, J.; Mayo, N.; Rometo, L. Macromol Symp 2007, 257, 71.
15. Monrabal, B.; Rometo, L.; Mayo, N.; Sancho-Tello, J. Macromol Symp 2009, 282, 14.
16. Muller, A. J. Prog Polym Sci 2005, 30, 559.
17. Beigzadeh, D.; Soares, J. B. P.; Duever, T. A. J Appl Polym Sci 2001, 80, 2200.
18. Zhang, F. J.; Liu, J. P.; Fu, Q.; Huang, H. Y.; Hu, Z. J.; Yao, S. J Polym Sci Part B: Polym Phys 2002, 40, 813.
19. Zhang, F. J.; Fu, Q.; Lu, T. J.; Huang, H. Y.; He, T. B. Polymer 2002, 43, 1031.
20. Virkkunen, V.; Laari, P.; Pitkanen, P.; Sundholm, F. Polymer 2004, 45, 4623.
21. Muller, A. J.; Hernandez, Z. H.; Arnal, M. L.; Sanchez, J. J. Polym Bull 1997, 39, 465.
22. Sun, X.; Shen, H.; Xie, B.; Yang, W.; Yang, M. Polymer 2011, 52, 2, 564.
23. Virkkunen, V.; Laari, P.; Pitkanen, P.; Sundholm, F. Polymer 2004, 45, 3091.
24. Zerbi, G.; Ciampelli, F.; Zamboni, V. J Polym Sci 1963, C7, 141.
25. Kissin, Y. V.; Rishina, L. A. Eur Polym J 1976, 12, 10, 757.
26. Kang, J.; Chen, J. Y.; Cao, Y.; Li, H. L. Polymer 2010, 51, 1, 249.
27. An, H.; Zhao, B.; Ma, Z.; Shao, C.; Wang, X.; Fang, Y.; Li, L.; Li, Z. Macromolecules 2007, 40, 4740.
28. Kissin, Y. V.; Tsvetkova, V. I.; Chirkov, N. M. Vysokomol Soedin 1968, A10, 1092.
29. Kissin, Y. V. Adv Polym Sci 1975, 15, 92.
30. Miyamoto, T.; Inagaki, H. J. Polym Sci 1969, A2, 7, 963.
31. Zhu, X. Y.; Yan, D. Y.; Yao, H. X.; Zhu, P. F. Macromol Rapid Commun 200, 21, 7, 354.
32. Zhu, X. Y.; Yan, D. Y. Macromol Chem Phys 2001, 202, 7, 1109.
33. Zhu, X. Y.; Li, Y.; Yan, D. Y.; Zhu, P.; Lu, Q. Colloid Polym Sci 2001, 279, 292.
34. Zhu, X. Y.; Yan, D. Y.; Fang, Y. P. J Phys Chem B 2001, 105, 12461.
35. Stolarski, L. Polimery 2005, 50, 894.
36. Busico. V.; Cipullo, R.; Monaco, G.; Talarico, G.; Vacatello, M.; Chadwick, J. C.; Segre, A. L.; Sudmeijer, O. Macromolecules 1999, 32, 4173.
37. Busico, V.; Cipullo, R. Prog Polym Sci 2001, 26, 443.
38. Fillon, B.; Wittmann, J. C.; Lotz, B.; Thierry, A. J Polym Sci Polym Part B: Polym Phys 1993, 31, 1383..
39. Fillon, B.; Lotz, B.; Thierry, A.; Wittman, J. C. J Polym Sci Part B: Polym Phys 1993, 31, 1395.
40. Fillon, B.; Thierry, A.; Wittman, J. C.; Lotz, B. J Polym Sci Part B: Polym Phys 1993, 31, 1407.
41. Gedde, U. W. Polymer Physics. London: Chapman and Hall, 1995; p 144.
42. Bond, E. B.; Spruiell, J. E.; Lin, J. S. J Polym Sci Part B: Polym Phys 1999, 37, 3050.
43. Iijima, M.; Strobl, G. Macromolecules 2000, 33, 5204.
44. Keating, M. Y.; Lee, I. H.; Wong, C. S. Thermochim Acta 1996, 284, 47.
45. Paolini, Y.; Ronca, G.; Feijoo, J. L.; Silva, E. D.; Ramirez, J.; Muller, A. J. Macromol Chem Phys 2001, 202, 1539.
46. Brandrup, J.; Immergut, E. H. Polymer Handbook, 3rd ed.; Wiley-Interscience: New York, 1989; p 27.
47. Paukkeri, R.; Vaananen, T.; Lehtinen, A. Polymer 1993, 34, 2488.